Aging effect of diethanolamine derived precursor sol on TiO_2 films deposited at different annealing temperatures

Amita Verma · M. Kar · D. P. Singh

Abstract A diethanolamine stabilized precursor sol has been utilized for studying the effect of sol aging and annealing temperature on key properties of TiO_2 films. X-ray diffraction investigations have shown increased crystallite size in the films as a function of both sol aging and the thermal treatment. Fourier transform infrared studies have elucidated that cleavage of the bond involving diethanolamine and the alkoxide in the films requires high temperature annealing treatment upon the use of aged sol for the deposition of the films. Multiple step chronoamperometry has shown the ion storage capacity of the films increases as a function of sol aging, with the highest extent of Li ion insertion being obtained for films produced from as-prepared and aged sols and subsequently annealed at, 300 and 350 °C, respectively. Films with excellent optical quality were obtained. Ellipsometry revealed that the refractive indices of the films vary from 1.67 to 2.02. The highest thickness obtained in these films was nearly 900 nm. The bandgaps of the films for both direct and indirect transitions decreased as a function of precursor sol's aging. In addition, although the indirect bandgap values have shown a decrease with increasing annealing temperature, the direct bandgap values reveal a slight increase as a function of annealing temperature.

Keywords TiO_2 · Sol–gel · Annealing temperature · Aging · Optical bandgap · Refractive index · Porosity · Electrochemical characteristics

A. Verma (✉) · M. Kar · D. P. Singh
Electronic Materials Division, National Physical Laboratory, Dr. K. S. Krishnan Road, New Delhi 110012, India
e-mail: amitaverma75@gmail.com

1 Introduction

Titanium dioxide has many interesting physical properties, which make it suitable for thin film applications. Because of their good transmittance in the visible region, high refractive index, and chemical stability, TiO_2 films have found wide application for various optical coatings [1–4]. The high dielectric constant of TiO_2 (the largest H among simple metal oxides) opens prospects for the use of TiO_2 thin films in microelectronic devices, e.g. in capacitors or as a gate dielectric in metal-dielectric semiconductor devices [5, 6]. TiO_2 films have been suggested as photoanodes in the process of photoelectrolysis of water in solar energy conversion systems [7–9] and as electrochromic materials for display devices [9, 10]. Other numerous technological applications of TiO_2 coatings include its prospective use as a material for smart windows [11], antireflective coatings [12, 13], optical filters [14], in catalysis and solar cells. From the viewpoint of air and water purification, semiconductor photocatalyst TiO_2 has recently received wide interest due to its powerful oxidation strength, high photostability and low toxicity. The advantages of titania photocatalysis, such as low operation temperature, low cost and low energy consumption, have led the relevant applications to the stage of commercialization. TiO_2 is a wide band gap semiconductor ($E_g \sim 3.03$ eV and ~ 3.18 eV for the rutile and anatase phases, respectively) and the limited overlap with the solar spectrum (relatively low quantum yield) has limited its applications. Numerous studies have been focused on improving the photoresponse by dye sensitizing [15–20], depositing noble metals, surface modification, and doping. Dye-sensitized TiO_2 solar cells are a promising alternative for the development of a new generation of photovoltaic devices. TiO_2 films can be obtained by a large variety of

methods: thermal [21] or anodic [15] oxidation of titanium, electron beam evaporation [22], ion sputtering [23], chemical vapor deposition [7, 24], including plasma-enhanced chemical vapor deposition [25], and the sol–gel method [26–34].

Since the pioneering study in 1972 [35], titanium dioxide has been recognized as one of the most important electrode materials for semiconductor electrochemistry [36]. At normal pressure and temperature, three different TiO_2 crystalline structures are stable: rutile, anatase, and brookite. Li-doped TiO_2 (anatase) electrodes have demonstrated useful properties in photoelectrochemical solar cells and Li ion batteries [37, 38]. Regardless of the crystal structure, the Ti^{4+} ions are surrounded by six O_2^- creating the basic TiO_6 octahedral building block. Electrochromism in TiO_2 electrodes shows dependence on the crystalline structure with the anatase phase demonstrating this phenomenon. Although anatase films prepared by conventional methods are unable to intercalate Li ions to any significant extent, the nanoporous morphology of nanostructured films greatly facilitates reversible Li ion intercalation. Therefore, nanocrystalline coatings, due to their unique morphology and surface structure, are promising for Li ion intercalation. In a study comparing ion beam sputtered TiO_2 films with spin coated films deposited using titanium isopropoxide in ethanolic medium containing acetic acid, Ozer et al. [27] have reported higher optical quality in the latter films.

TiO_2 films have been previously prepared using different stabilizers such as acetic acid [26, 27, 39, 40], diethanolamine [31], hydrochloric acid [30], hydrogen peroxide solution [32] and acetylacetone [41] by various research groups. Ethanolamines [42–46] can yield very stable solutions for the oxides by controlling the rate of hydrolysis of the metal alkoxides. Diethanolamine and related chemicals are used as inhibitors for the precipitation of oxides on the hydrolysis of the alkoxides. The present study reports on the preparation of TiO_2 films by sol–gel spin coating, using precursor solutions employing diethanolamine as the stabilizing agent to prevent precipitation of titanium isopropoxide by ethanol. The main motivation of this work is to study the effect of sols aging and annealing temperature on the structural, optical, morphological and electrochemical characteristics of TiO_2 films. This study has provided information on the fact that in comparison to the aged sol, the as-prepared sol produces amorphous films even at relatively high annealing temperatures. In addition, the removal of additive and other remnant organic groups from the aged sol derived films requires higher annealing temperatures. This explanation is evidenced by the faint brown coloration observed in the aged sol derived films annealed at 200 and 300 °C.

2 Experimental

2.1 Preparation of sol

Titanium isopropoxide (TIP, Aldrich), anhydrous diethanolamine ($DEAH_3$, Loba Chemie) and anhydrous ethanol (C_2H_5OH, Merck) were used as the starting materials. The relative volume ratio of each chemical in the sol was TIP: $DEAH_3$: C_2H_5OH = 3:1:20. Mixing of the chemicals was carried out under ambient conditions. During the experimental process, the room temperature was (20 + 5) °C and the humidity remained at (60 + 10)%. Addition of TIP in ethanol prior to the introduction of diethanolamine induces immediate precipitation due to highly reactive alkoxide (TIP in the present study), therefore diethanolamine (1 mL), which was added as a stabilizing agent for hydrolysis was initially stirred with 10 mL of ethanol followed by the addition of TIP (3 mL). After magnetically stirring the solution for 15 min, the remaining ethanol (10 mL) w as added and the stirring w as continued for 45 min at room temperature. The sol was stable for a period of 3 weeks before it transformed into a gel. It has been observed that stirring the sol for a lesser duration significantly enhances the stability of the sol. In addition, the ambient humidity also greatly influences the gelation period of the sol. In low humidity conditions, the stability of the sol is significantly enhanced.

2.2 Preparation of TiO_2 thin films

Transparent fluorine doped tin oxide (SnO_2:F) coated glass substrates and micro slide glass were spin coated by the precursor sols at 3,000 rpm for 35 s. The films were annealed at 200, 300, 350 and 450 °C for 5 min and are uniform, transparent, and highly adherent to the substrates. The effect of sol aging on selected properties of the films was investigated. Sols both freshly prepared (as-prepared) and aged to the extent of just reaching the state of gelation have been used for the deposition of films. The aging time used to prepare the aged sol was 15 days. In principle, the presence of diethanolamine in the solution has led to a homogeneous solution without any precipitates. Under such conditions, the sol is stable for up to 3 weeks. Therefore, addition of diethanolamine is essential in order to retain highly transparent and reproducible coating solutions under the conditions employed in this study. In the absence of diethanolamine, the addition of ethanol to TIP induced rapid precipitation of TiO_2, and consequently the corresponding films were poorly adherent to the substrate and opaque. Thus, the films obtained without the stabilizer are not suitable as optical coatings and for electrochromic applications. This observation reflects the importance of the stabilizing agent in ensuring process reproducibility and in improving the adherence, transparency, and the quality of the films. In addition, the higher

viscosity of the aged sol due to increased degree of hydrolysis and condensation has produced thicker films.

2.3 Characterization of films

X-ray diffraction (XRD) patterns of the films have been recorded in the 2θ range from 8° to 70° with a D8 Advanced Bruker Diffractometer. Fourier Transform Infrared (FTIR) spectra of the films in the transmission mode have been recorded in the wavenumber range from 400 to 4,000 cm^{-1} on a Perkin-Elmer Model BX2 Spectrophotometer. The surface morphology of the films was observed using scanning electron microscopy (SEM) on a JEOL JSM 840 scanning electron microscope. The refractive indices, extinction coefficients, and thickness of the films have been determined using a Rudolph research null type manual ellipsometer at $\lambda = 546.1$ nm. The thicknesses of the films have also been measured directly with a stylus-based Talystep (Taylor Hobson) instrument. Transmission and reflection spectra of the films in the range 300–2,000 nm were recorded using a UV 3101 PC Shimadzu Spectrophotometer. Cyclic voltammetry (CV) studies have been performed on a computer controlled OMNI potentiostat. All measurements were performed in an electrolyte of 1 M $LiClO_4$/propylene carbonate in a three electrode arrangement comprising TiO_2 film as the working electrode, a platinum counter electrode and Ag/AgCl/KCl reference electrode. The CV experiments were conducted at a scan rate of 20 mV s^{-1} and the potential was swept between cathodic (−1.5 V) and anodic (+1.5 V) versus Ag/AgCl/KCl. Electrochemical measurements on the TiO_2 electrodes versus platinum in the liquid electrolyte have been carried out on a computer controlled setup consisting of a He–Ne laser source ($\lambda = 632.8$ nm), a Si photodetector together with a versatile micro-controller based electrochromic device (ECD) characterization unit. Multiple step potential cycling was performed by applying square wave potential of amplitudes +2.0 and +3.5 V at a frequency of 0.0011 Hz. Transmission profiles in the colored and bleached states have been obtained in situ in a two-electrode electrochemical cell (built with two flat fused quartz windows) comprising TiO_2 films and platinum counter electrode with application of a constant current density of 1 mA cm^{-2} for 3 min.

3 Results and discussion

3.1 Structural analysis

3.1.1 X-ray diffraction

X-ray diffraction (XRD) patterns of the films are illustrated in Fig. 1. It is confirmed from the results that the

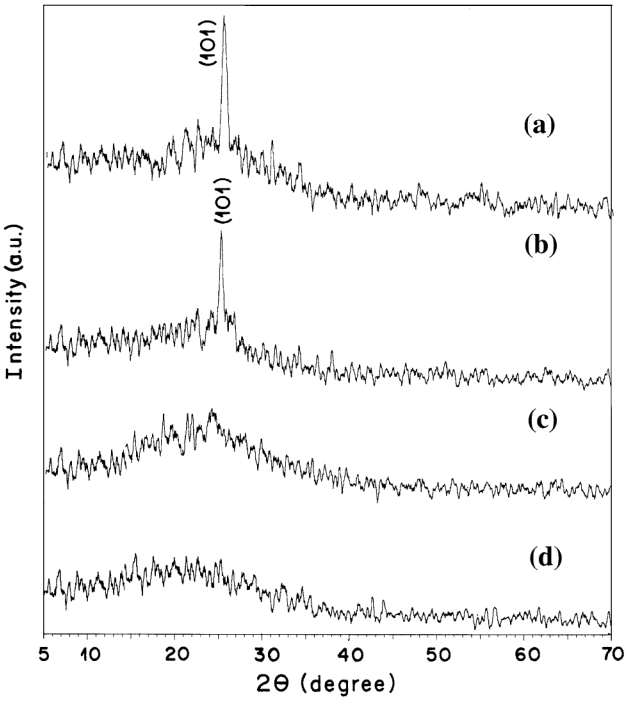

Fig. 1 X-ray diffraction patterns of TiO_2 films deposited from the aged sol and heated at different temperatures. (*a*) 450 °C, (*b*) 350 °C, (*c*) 300 °C, and (*d*) 200 °C

crystallinity in the films is improved by depositing the films from relatively aged sols and in order to attain crystallinity in the film obtained from the as-prepared sol, higher annealing temperatures are required. The films prepared from the as-prepared sol are amorphous at all annealing temperatures. Significantly, the films deposited using aged sols exhibit the presence of a crystalline phase at and above 350 °C. The crystalline phase observed in these films is identified as the tetragonal anatase phase oriented along the (101) plane [28]. The nano-scaled crystallite sizes measured by the Debye Scherer formula are listed in Table 1. Wang et al. [32], in their spin coated TiO_2 films deposited using a poly-peroxotitanic acid, obtained amorphous coatings at 250 °C and crystalline coatings at 350 °C and above. The authors' data also revealed an increase in grain size with increasing annealing temperature. In our case, the threshold temperature for the appearance of crystallinity in the films is also observed at 350 °C. Vorotilov et al. [28] in their XRD investigations studied the evolution of crystallinity in the films deposited from an acidic solution of titanium alkoxide in alcohol and showed the presence of diffraction peaks assigned to the anatase phase at 400 and 600 °C. The coexistence of rutile and anatase phases, however, has been reported by these authors at 800 °C. In the present work, the presence of rutile could not be detected in the films because the highest annealing temperature employed in the work was 450 °C. Ozer et al.

Table 1 Crystallite size, ion storage capacity (ISC) and diffusion coefficient (D) of the TiO_2 films deposited at different annealing temperatures from the as-prepared (1) and aged sol (2)

Annealing temperature (°C)	Crystallite size (nm) (1)	Crystallite size (nm) (2)	ISC (mC cm^{-2}) (1)	ISC (mC cm^{-2}) (2)	D × 10^{-11} (cm^2 s^{-1}) (1)	D × 10^{-11} (cm^2 s^{-1}) (2)
200	–	–	9.6	18.6	0.05	0.39
300	–	–	20.1	21.3	2.19	2.49
350	–	11.0	15.1	28.2	0.37	2.49
450	–	16.5	15.5	21.6	2.29	23.27

[26, 47] employed the spin coating technique and prepared amorphous gel coatings below 400 °C and crystalline films above 400 °C. TiO_2 films obtained using acetic acid stabilizer at 70 °C by Ozer et al. [26] were amorphous and free from pinholes or microcracks. In addition, TiO_2 films annealed at 450 °C deposited using acetic acid stabilizer by Ozer [39] were also crystalline. TiO_2 films annealed at 480 °C (film thickness: 230 nm) deposited using diethanolamine stabilizer by Dinh et al. [31] were crystalline with an average grain size of 38 nm. In the case of TiO_2 films deposited using hydrochloric acid, the threshold temperature for the onset of crystallization in the films was observed at 350 °C by Hu et al. [30]. TiO_2 films prepared by Buscema et al. [41] using acetylacetone stabilizer were crystalline at and above 400 °C.

3.1.2 Fourier transform infrared (FTIR) spectroscopy

FTIR studies have shown that major structural changes take place in the films as a result of sol aging. For example, in the films deposited from the as-prepared sol, the removal of diethanolamine and other remnant organic groups is easier due to the lesser degree of complexation between diethanolamine and Ti^{4+} metal ion (diethanolamine interacts with titanium alkoxide as a tridentate ligand [42, 48]). The possible reaction between diethanolamine and Ti isopropoxide can be represented as shown below:

$$\mathrm{Ti}\left(\mathrm{OPr^i}\right)4 + \mathrm{DEAH_3} \rightarrow \mathrm{Ti(DEA)}\left(\mathrm{Pr^iO}\right) + 3\left(\mathrm{Pr^iOH}\right). \quad (1)$$

Due to the greater degree of hydrolysis and condensation during sol aging, the increased formation of organic byproducts leads to the requirement of higher annealing temperature for their elimination. The aforesaid discussion is quantified by the band positions observed in the different films. In comparison to the as-deposited (unannealed) film, which exhibits bands assigned respectively to ν(O–H), δ(O–H), C–H deformation, ν(C–O), ν(Ti–O) [49] and ν(Ti–O–Ti) [50] modes at 3,490, 1,658, 1,434, 1,082, 798 and 530 cm^{-1} the 200, 300, 350 and 450 °C annealed films deposited from the as-prepared sol exhibit only vibrational bands assigned to ν(Ti–O), ν(Ti–O–Ti) and ν(O–H) modes near 550, 798 and 3,500 cm^{-1}, respectively. The only difference between the abovementioned annealed films is the slight variations in the relative intensities of the ν(Ti–O) and ν(Ti–O–Ti) bands. In contrast, major structural changes are observed in the films deposited using the aged precursor sol. Indeed, diethanolamine is only completely decomposed in these films upon treating the films thermally at 450 °C, and bands signifying the presence of diethanolamine are still clearly evident in the films annealed at 200, 300 and 350 °C. For instance, in the film deposited from the aged sol and subsequently annealed at 200 °C, the bands ascribed to ν(C–O) (diethanolamine) and δ(C–H) modes (isopropoxy) at 1,102 cm^{-1} [51] and 1,444 cm^{-1} [52], respectively, are highly intense (Fig. 2). In the films annealed at 300 and 350 °C, these bands exhibit weak intensity and they are no longer evident in films treated at 450 °C. It is thus clearly exemplified by FTIR that a higher processing temperature is required in the case of the films deposited from the aged sol to ensure complete removal of the organic byproducts.

3.2 Morphological properties

Figures 3 and 4 show the SEM micrographs of the different films. It is evident from the micrographs that the films produced from the aged sol have reduced porosity, which is attributed to an increased crystallite size which promotes densification in the films. The SEM micrographs also reveal that the granular nature of the films becomes well defined upon increasing the annealing temperature. The largest particle sizes observed for the films deposited from the as-prepared and the aged sols are 250 and 330 nm, respectively. The pore size was observed to lie in the 100–166 nm range (Table 2). In the present work, the effect of annealing temperature on porosity in the films was less pronounced than the influence of sol aging. This is further demonstrated by the refractive indices measurements carried out using ellipsometry (see below). In addition, it was observed that porosity variations in the films have

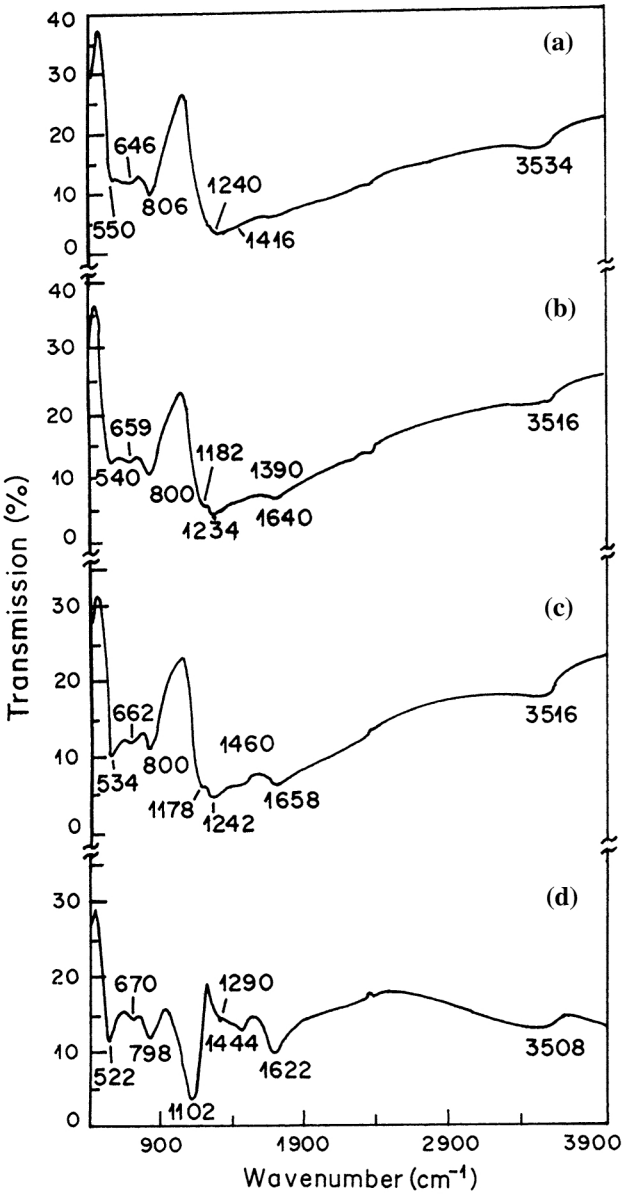

Fig. 2 FT-IR transmission spectra of TiO_2 films deposited from the aged sol and annealed at different temperatures. (*a*) 450 °C, (*b*) 350 °C, (*c*) 300 °C, and (*d*) 200 °C

influenced their electrochemical activities (as also discussed below).

3.3 Optical properties

Reflection spectra (300–2,000 nm) of the various films are presented in Fig. 5. The corresponding transmission characteristics of the films deposited using the as-prepared sol are superior to that deposited from the aged sol. This is due to the greater thickness of the latter films (which is a consequence of the greater degree of hydrolysis/condensation and associated higher viscosity of the aged sol). As expected, increasing annealing temperature led to a corresponding decrease in the thickness of the films, which varied from 200 to 900 nm depending on the aging of the sol and the annealing temperature. In addition, the differences in the reflectivity characteristics of the samples are a consequence of their varying refractive indices. Also, in general, the decrease in transmission of the films in the solar spectral range is accompanied by a corresponding increase in their reflection characteristics, indicating that the films are weakly absorbing. Overall, the films exhibit high optical quality due their excellent transmittance, uniform texture, and low extinction coefficient values. High transmittance in the films is a prerequisite for their application in transmissive electrochromic devices. Anatase is known to possess a refractive index of 2.52 [53]. Using $Ti(OC_2H_5)_4$, C_2H_5OH, H_2O and HCl to produce anatase films, Vorotilov et al. [28] have observed refractive indices in the range of 1.7–2.3 for processing temperatures between 200 and 900 °C (1.9 and 2.05 at 400 and 500 °C, respectively). In addition, these authors have also reported an increase in refractive index with increasing crystallite size. Ozer [39] reported respective refractive indices of 1.84 and 2.41 for amorphous and crystalline TiO_2 films produced from an acetic-acid-stabilized sol. In the present study, the index of refraction varies within the relatively narrow range from 1.83 to 1.89 for films deposited from the as-prepared sol and annealed at different temperatures. In contrast, films prepared from aged sols exhibited significant variations in refractive index (from 1.67 to 2.02) with increasing calcination temperature, consistent with the significant variations in structure and composition occurring in this latter system during heating at 350 and 450 °C (see above). The calculated values of refractive index (n) at the wavelength corresponding to transmittance maxima and minima have been fitted with a Levenberg–Marquardt regression algorithm to the following dispersion relation:

$$n(\lambda) = A + B/\lambda^2 + C/\lambda^4, \quad (\text{with } \lambda \text{ in } \mu m) \text{ giving}$$

$$A = 2.109$$

$$B = -1.504 \times 10^{-2}$$

$$C = 6.71 \times 10^{-3}$$

The film thickness, refractive index, and extinction coefficient values of the films are summarised in Table 2. From Table 2 it is evident that the variations in refractive index and extinction coefficient values are not systematic, presumably due to the fact that the major structural changes are occurring in the aged-sol-derived films at different annealing temperatures. Amongst the aged-sol-derived films, the lowest refractive index was observed for the film heated at 350 °C (1.67), while the film heated at 450 °C exhibited the highest value (2.02). These large variations in refractive indices are attributed to variations in sample

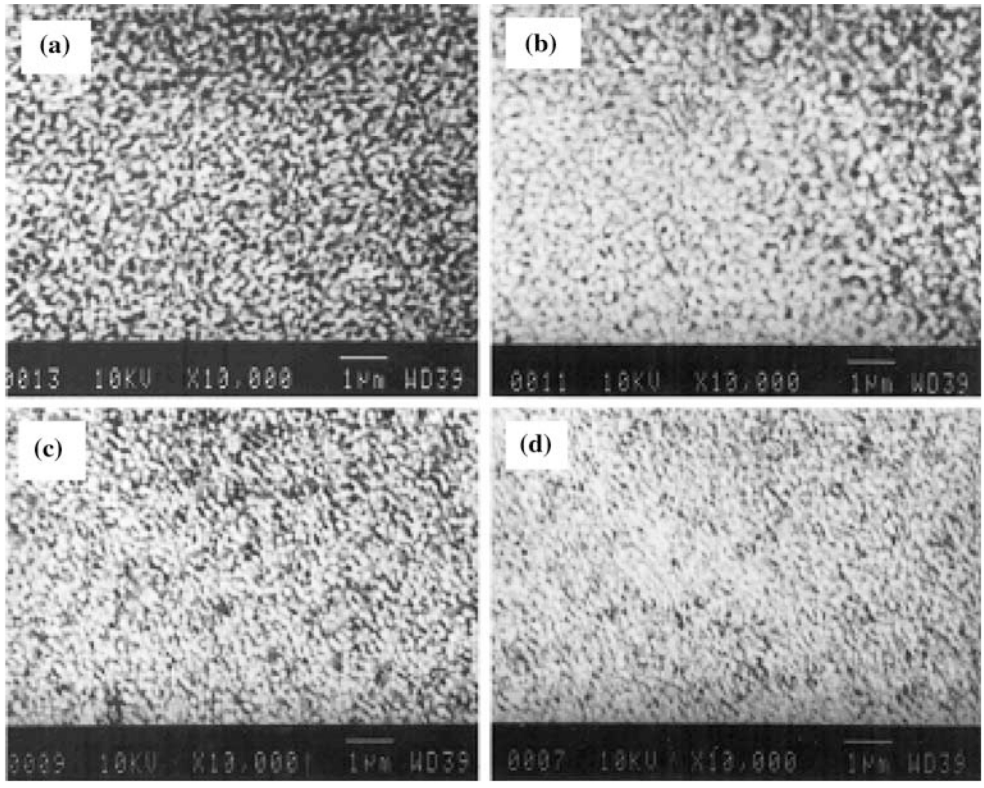

Fig. 3 SEM micrographs of TiO_2 films deposited from the as-prepared sol and annealed at different temperatures. **a** 450 °C, **b** 350 °C, **c** 300 °C, and **d** 200 °C

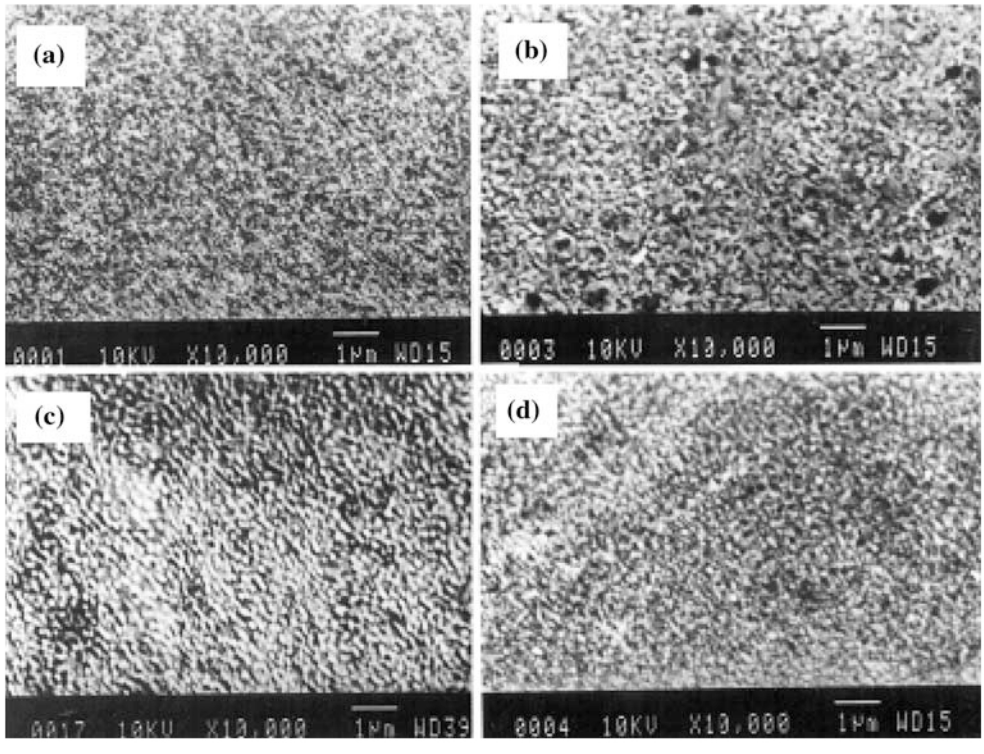

Fig. 4 SEM micrographs of TiO_2 films deposited from the aged sol and annealed at different temperatures. **a** 450 °C, **b** 350 °C, **c** 300 °C, and **d** 200 °C

Table 2 Film thickness (d), refractive index (n), extinction coefficient (k) and pore size of the TiO_2 films deposited at different annealing temperatures from the as-prepared (1) and aged sol (2)

Annealing temperature (°C)	d (nm) (1)	d (nm) (2)	n (1)	n (2)	k (1)	k (2)	Pore size (nm) (1)	Pore size (nm) (2)
200	600	700	1.875	1.800	0.290	0.060	150	105
300	500	900	1.835	1.910	0.190	0.024	166	120
350	300	900	1.850	1.675	0.200	0.460	125	140
450	200	250	1.890	2.020	0.160	0.080	100	110

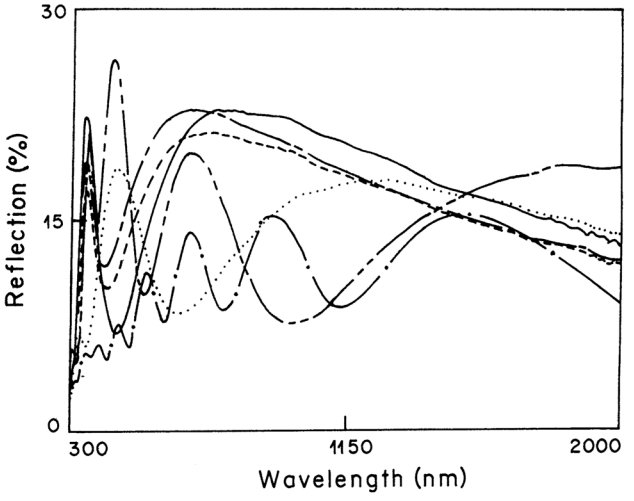

Fig. 5 Reflection spectra of TiO_2 films deposited from the as-prepared and aged sols and annealed at different temperatures (as-prepared) 200 °C (…), (as-prepared) 300 °C (—), (as-prepared) 350 °C (- - -), (as-prepared) 450 °C (– - –), (aged) 200 °C (–·–) and (aged) 450 °C (– - - –)

stoichiometry and the volume fraction of pores in the two samples. Furthermore, the relatively high extinction coefficient (0.46) of the 350 °C annealed film reveals its highly absorbing nature. In contrast, the significantly lower extinction coefficient value (0.08) of the 450 °C annealed film suggests that it would be more suitable as an optical coating.

3.3.1 Energy bandgaps of TiO_2 films

For a transparent thin film, the absorption coefficient per unit length (D) is determined from its transmittance (T), i.e.

$$\alpha = \ln(1/\mathrm{T})/d \tag{2}$$

where d is the film thickness. If the film is semiconducting, a relationship exists between α and the energy bandgaps (E_g) for direct and indirect transitions [54, 55]. It follows

$$A/d = \alpha = \left(h\nu - E_g\right)^{\gamma} \tag{3}$$

where A is the absorption coefficient, $\gamma = 1/2$ or 2 for direct and indirect transitions, respectively. According to Eqs. 1 and 2, by extrapolating the linear part of a curve of A^{γ} versus photon energy to the abscissa, the energy bandgaps for indirect and direct transition can be derived. The effect of annealing temperature and sol aging on the direct and indirect bandgaps of the films is shown in Figs. 6 and 7, respectively. These data reveal that the bandgaps for both direct and indirect transitions decrease with increasing aging of the sol. Quantitatively, the direct and indirect bandgaps for the films deposited from as-prepared/aged sols are 4.05/3.80 and 3.47/3.35, respectively. These values are comparable to the literature data of 3.65 and 3.08 eV, respectively, for an anatase film heated at 400 °C [55]. The red shift of the bandgap with aging of the precursor sol is attributed to the associated increase in grain size. The film deposited from the as-prepared sol contains randomly-oriented smaller grains. The higher concentration of grain boundaries in such a film leads to a broadening of the absorption band edge and consequently shifts the bandgap towards higher energies. The effect of processing temperature on the direct and indirect bandgaps has also been studied for the films. From Figs. 6 and 7, it is evident that the bandgap for indirect transitions decreases with increasing temperature. In particular, the film heated at 200 °C exhibited an indirect bandgap of 3.75 eV, while

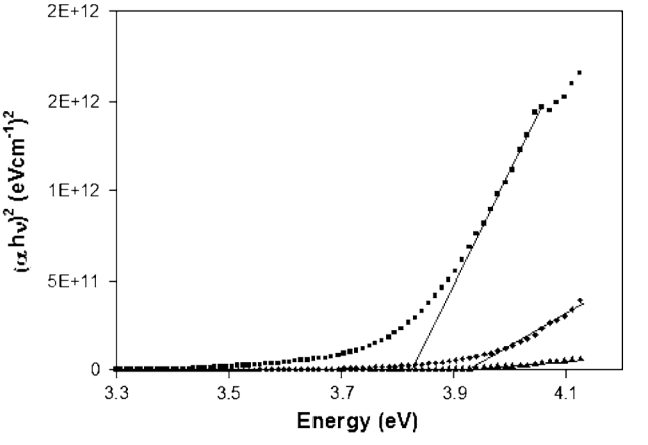

Fig. 6 Direct bandgap evaluation from linear dependence of $(\alpha h\nu)^2$ versus photon energy for the TiO_2 films. (as-prepared sol) 200 °C (*filled triangle*), (as-prepared sol) 450 °C (*filled diamond*) and (aged sol) 450 °C (*filled square*)

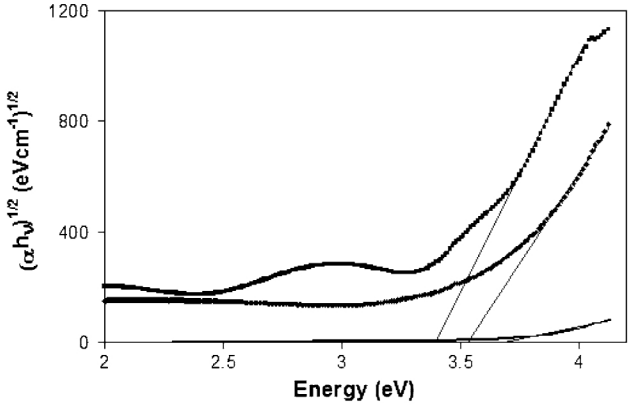

Fig. 7 Indirect bandgap evaluation from linear dependence of $(\alpha h\nu)^{1/2}$ versus photon energy for the TiO_2 films. (as-prepared sol) 200 °C (—), (as-prepared sol) 450 °C (*filled diamond*) and (aged sol) 450 °C (*filled square*)

heat-treatment at 450 °C yielded films with an indirect bandgap of 3.50 eV. In contrast, the direct bandgap exhibits a slight increase with increasing temperature, with heating at 200 and 450 °C yielding direct bandgaps of 3.90 and 3.95 eV, respectively. The films prepared at lower temperatures exhibit a wide bandgap or show a blue shift of the optical bandgap as a consequence of exciton confinement due to decreased grain size. Furthermore, the optical bandgap of the films in the present work was found to be independent of the film thickness.

3.4 Electrochemical investigations

To determine the capacity of the films to reversibly intercalate and deintercalate Li ions, cyclic voltammetry has been employed. Figs. 8 and 9 show the cyclic voltammograms (CVs) of the films within a + 1.5 V potential range at a scan rate of 20 mV s^{-1}. These data clearly demonstrate that the films produced from the aged sol exhibit superior electrochemical activity. In particular, the diffusion coefficients for the films measured using the cathodic peak current densities from the Randles–Sevcik equation (below), which are summarized in Table 1, are up to 10 times higher in the coatings produced from the aged sols.

$$\mathrm{Ip} = 0.4463\,\mathrm{nF}(\mathrm{nF/RT})^{1/2}\mathrm{CD}^{1/2}\mathrm{V}^{1/2} \qquad (4)$$

Here, Ip = peak current density (A cm^{-2}), n = number of electrons involved in the redox reaction, F = Faraday constant, R = gas constant, T = temperature, C = concentration of Li^+ in the liquid electrolyte (mol cm^{-3}), v = scan rate (V s^{-1}), D = diffusion coefficient (cm^2 s^{-1}).

From the shapes of the CVs, it is also evident that significant variations have occurred in the cathodic and anodic sweeps with variations in sol aging and heating

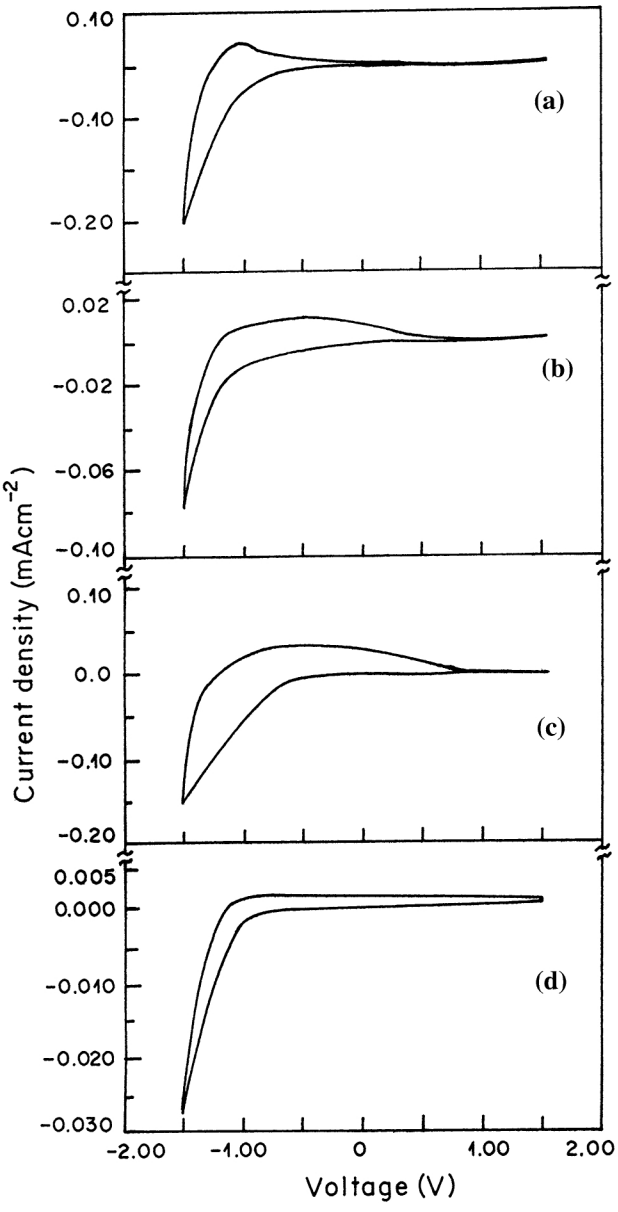

Fig. 8 Cyclic voltammograms of TiO_2 films deposited from the as-prepared sol and annealed at different temperatures. **a** 450 °C, **b** 350 °C, **c** 300 °C, and **d** 200 °C at a scan rate of 20 mV s^{-1}

temperature of the films. Electrochemical reactions involve the transfer of ions within the film and they depend upon the number of active insertion sites available. These events are related to the film thickness. A thicker film contains a larger number of active insertion sites and as the aged sol film is thicker, the diffusion of Li ions would be expected to be more facile. Consistent with this interpretation, the diffusion coefficients for the films produced from the aged sols are higher at all annealing temperatures (Table 1). In addition, it is typically observed that an increase in the crystallinity of such films enhances their electrochemical response. The ion-storage capacity (ISC), defined as the

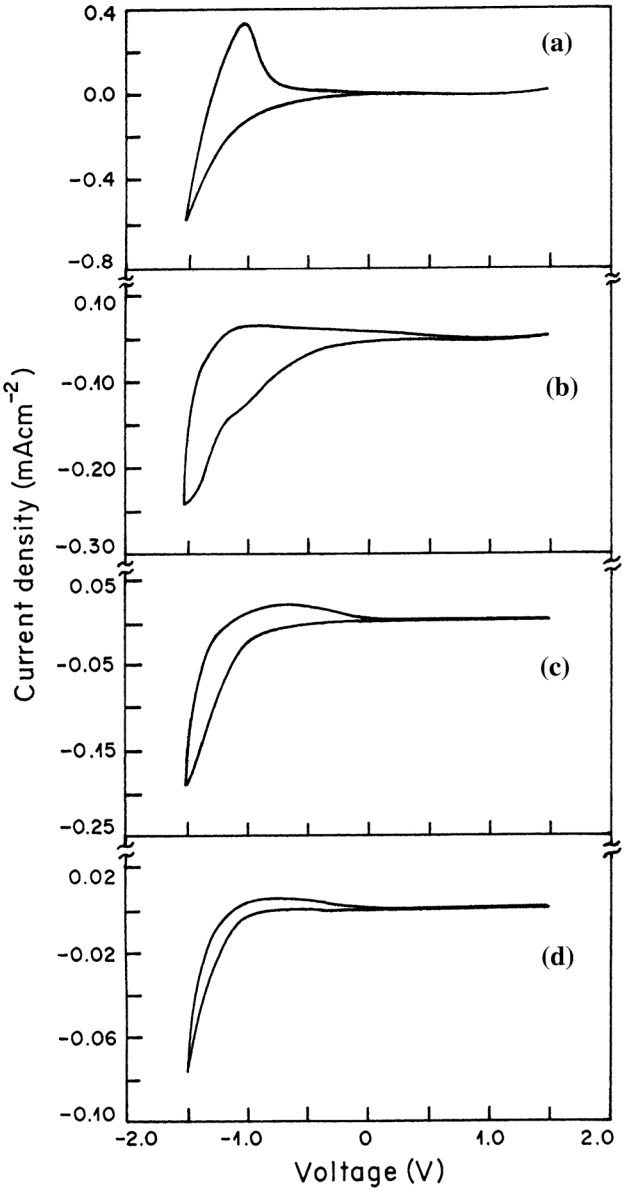

Fig. 9 Cyclic voltammograms of TiO_2 films deposited from the aged sol and annealed at different temperatures. **a** 450 °C, **b** 350 °C, **c** 300 °C, and **d** 200 °C at a scan rate of 20 mV s^{-1}

quantity of Li^+ inserted per unit area of active TiO_2 electrode (Table 1), was investigated using a two-electrode electrochemical cell which incorporated the TiO_2 films as one electrode, a Pt counter electrode and a 1 M $LiClO_4$/propylene carbonate electrolyte with application of +2.0 V. The ISC of the films increased with the aging of the sol, consistent with superior electrochemical activity compared to those produced from the as-prepared (fresh) sol. The highest ISC values were obtained for films from the as-prepared and aged sols following firing at 300 (20.1 mC cm^{-2}) and 350 °C (28.2 mC cm^{-2}), respectively. The electrochemical characteristics of the films are well correlated with their porosity (and refractive indices), with these two films exhibiting the lowest refractive indices (1.83 and 1.67, respectively) and highest porosity. This establishes the importance of porosity in modulating the electrochemical activity of the films and demonstrates that an optimum heating program is necessary to enhance their electrochemical response. It is evident from the above discussion that the ion storage capacity depends upon a number of parameters, including: (1) the number of active insertion sites available for the electrochromic reactions; (2) the film thickness, since the electrochromic reaction is not a surface reaction but involves the transfer of ions within the bulk of the film; (3) porosity; and (4) crystallite size. Amorphous mesoporous films exhibited higher ion storage capacities, and since a thicker film was obtained from the aged sol (which contains a larger number of active insertion sites), its capacity to intercalate Li^+ ions is greater. The electrochromic characteristics of these films have also been examined. Consistent with the observation that a larger extent of Li^+ ion insertion results in greater coloration efficiency in the films, a higher electrochromic response was evident in the films having the highest ion storage capacities.

4 Conclusions

TiO_2 films with high optical quality have been deposited using a transparent diethanolamine derived precursor sol. The effect of annealing temperature and aging of the sol on key properties of the films has been investigated. XRD has revealed an increase in the degree of crystallinity in the films as a function of precursor sol aging and thermal treatment temperature. FTIR investigations have revealed that higher processing temperatures are required for the films deposited from the aged sol to ensure complete decomposition of the diethanolamine and other organic species. The bandgaps of the films for both direct and indirect transitions decreased with increasing aging of the sol. Higher porosities, an increase in the number of active insertion sites and increasing thickness resulted in enhanced electrochemical activity. The electrochemical response of the films was found to be modulated by both the aging of the precursor sol and the annealing temperature, with aging and an optimized heating temperature leading to significantly improved electrochemical performance. This study has shown that the films derived from the aged sol always exhibit good response, although treatment of the films at an optimum temperature is also an important prerequisite for obtaining films suitable for electrochromic applications.

Acknowledgments Financial support from the Indian Council of Scientific & Industrial Research (AV) and access to the characterization facilities provided by the University Science Instrumentation Center, University of Delhi, are gratefully acknowledged.

References

1. Schroder H (1969) In: Haas G, Thun RE (eds) Physics of thin films, vol 5. Academic, New York, p 87
2. Pulker HK (1984) Thin film science and technology vol 6, coatings on glass. Elsevier, Amsterdam
3. Yoldas BE, O'keefe TW (1979) Appl Opt 18:3133
4. Yoldas BE (1982) Appl Opt 21:2966
5. Fuyuki T, Matsunami H (1986) Jpn J Appl Phys 25:1288
6. Bertrand PA, Fleischauer PD (1983) Thin Solid Films 103:167
7. Yoko T, Kamiya K, Yuasa A, Tanaka K, Sakka S (1988) J Non Cryst Solids 10:483
8. Doeuff S, Henry M, Sanchez C (1986) MRS Symp Proc 73:653
9. Livage J (1986) MRS Symp Proc 73:717
10. Nabavi N, Doeuff S, Sanchez C, Livage J (1989) Mater Sci Eng B 3:203
11. Dislich H, Hinz P (1982) J Non Cryst Solids 48:11
12. Yoldas B (1980) Appl Opt 19:1425
13. Dislich H (1988) In: Lein LK (ed) Sol-gel technology for thin films. Noyer, Park Ridge, p 67
14. Phillips RW, Dodds JW (1981) Appl Opt 20:40
15. Morris B, Enry H (1978) US Patent 4, 200, 474
16. Regan BO, Gratzel M (1991) Nature 353:737
17. Gratzel M (2001) Nature 414:338
18. Kay A, Gratzel M (1996) Sol Energy Mater Sol Cells 14:99
19. Gomez MM, Lu J, Solis JL, Olsson E, Hagfeldt A, Granqvist CG (2000) J Phys Chem B 104:8712
20. Gomez MM, Magnusson E, Olsson E, Hagfeldt A, Lindquist S-E, Granqvist CG (2000) Sol Energy Mater Sol Cells 62:259
21. Kozlowski MR, Tyler PS, Smyrl WH, Atanasoski RT (1989) J Electrochem Soc 136:442
22. Lottiaux M, Boulesteix C, Nihoul G (1989) Thin Solid Films 170:107
23. Bellan B (1983) J Non Cryst Solids 55:405
24. Yeung KS, Lam YW (1983) Thin Solid Films 109:169
25. Williams LM, Hess DW (1983) J Vac Sci Tech A 1:1810
26. Ozer N, Tepehan F, Bozkurt N (1992) Thin Solid Films 219:193
27. Ozer N, Demiryonta H, Simmons JH (1991) Appl Opt 30:3661
28. Orotilov KAV, Orlova EV, Petrovsky VI (1992) Thin Solid Films 207:180
29. Kohno K (1992) J Mater Sci 27:658
30. Hu L, Yoko T, Kozuka H (1992) Thin Solid Films 219:18
31. Dinh NN, Oanh NThT, Long PD, Bernard MC, Hugot-Le Goff A (2003) Thin Solid Films 423:70
32. Wang Z, Hu X (1999) Thin Solid Films 352:62
33. Stanger UL, Orel B, Regis A, Colomban PH (1997) J Sol Gel Sci Tech 8:965
34. Mendez-Vivar J, Mendoza-Serna R, Gomez-Lara J, Gavino R (1997) J Sol Gel Sci Tech 8:235
35. Fujischima A, Honda K (1972) Nature 238:37
36. Finklea HO (1988) In: Finklea HO (ed) Semiconductor electrodes. Elsevier, Amsterdam, p 49
37. Regan BO, Gratzel M (1991) Nature 353:373
38. Huang SY, Kavani L, Gratzel M, Exnar I (1995) J Electrochem Soc 142:142
39. Ozer N (1992) Thin Solid Films 214:17
40. Mendez-Vivar J, Brinker CJ (1994) J Sol Gel Sci Tech 2:393
41. Buscema CL, Malibert C, Bach S (2002) Thin Solid Films 418:79
42. Singh A, Mehrotra RC (2004) Coord Chem Rev 248:101
43. Sharma M, Singh A, Mehrotra RC (1999) Polyhedron 18:77
44. Kemmitt T, Ai-Salim NI, Gainsford GJ (2000) Inorg Chem 39:6067
45. Sharma MK, Singh A, Mehrotra RC (2001) Ind J Chem A 40:568
46. Sharma MK, Singh A, Mehrotra RC (2001) Synth React Inorg Met Org Chem 31:371
47. Ozer N, Chen DG, Simmons J-H (1991) Ceram Trans 20:253
48. Rao CNR (1963) Chemical applications of infrared spectroscopy. Academic Press, New York, London, p 188
49. Kullman L, Azens A, Granqvist CG (1997) J Appl Phys 81:8002
50. Larbot A, Laaziz I, Marignan J, Quinson JF (1992) J Non Cryst Solids 147–148:157
51. Yamamoto A, Kambara S (1957) J Am Chem Soc 79:4344
52. Mendez-Vivar J, Campero A, Livage J, Sanchez C (1990) J Non Cryst Solids 121:26
53. Kingery WD, Bowen HK, Uhlmann DR (1976) Introduction to ceramics. Wiley, New York, p 669
54. Sze SM (1981) Physics of semiconductor devices, 2nd edn. Wiley, New York
55. Aoki A, Nogami G (1996) J Electrochem Soc 143:L191